Supporting Information

Shelterin components modulate nucleic acids condensation and phase separation in the context of telomeric DNA

Andrea Soranno, J. Jeremías Incicco, Paolo De Bona, Eric J. Tomko, Eric A. Galburt, Alex S. Holehouse and Roberto Galletto

Fluorescence recovery after photobleaching (FRAP) determinations.

In order to monitor the diffusion of either TRF2 or DNA within condensates we performed fluorescence recovery after photobleaching (FRAP) experiments on selected TRF2-DNA droplets. Measurements were performed by focusing inside the droplets and photobleaching a limited area of the droplet determined by the size of the illuminated volume at the corresponding laser power.

Samples contained either fluorescently label protein or fluorescently label DNA. 30 µL samples were prepared in 1.5 mL-plastic test tubes at room temperature. For samples containing fluorescently labeled protein, unlabeled protein was first premixed with its labeled counterpart in the corresponding final buffer and salt concentration, and then was mixed with DNA. For fluorescently labeled DNA, this was first premixed with its unlabeled counterpart and then mixed with protein. Within 10 min after mixing, 0.5 µL of 0.1 % v/v Tween20 and 0.5 µL of beta-mercapthoethanol were added, to reduce nonspecific sticking to cuvette walls and increase photostability[1], respectively, and samples were mixed and pipetted into plastic low binding tubes.
Otherwise indicated, fluorescence measurements were performed on samples containing either fluorescein (FAM) 3'-labeled DNA or Alexa Fluor 488 labeled full length TRF2, at a total concentration of 50 nM labeled material mixed with the concentrations of unlabeled DNA and protein indicated for each experiment.

Pre- and post-photobleaching signals were recorded with an excitation power of 8 and 40 nW for FAM-labeled DNA and Alexa Fluor 488 labeled TRF2, respectively. Photobleaching of focused spots inside the droplets was accomplished by 1 minute irradiation at 20 µW for FAM-labeled DNA and at 100 µW for Alexa Fluor 488 labeled TRF2. Representative FRAP traces showed in *Results* correspond to individual time traces time-binned with 100 ms binwidth. All experiments were performed at room temperature.

FRAP analysis – To analyze FRAP traces and obtain the extent of recovery and mean diffusion times we employed the 3-dimensional FRAP formalism described by Blonk *et al*[2] solved for the condition of no scanning. According to this formalism, the relative fluorescence signal,

$$\Delta F_{rel}(t) = \frac{F(t)-F_{bkg}}{F_{pre}-F_{bkg}} \qquad \text{(eq. S1)}$$

where F(t), F_{bkg} and F_{pre} are respectively the time dependent fluorescence intensity recorded after photobleaching, the background recorded from buffer alone and the fluorescence recorded before photobleaching, for the case of a single diffusing species is described by:

$$\Delta F_{fit}(t) = \Delta F_{max}(t)\left[1 + 0.5\left(1 - exp\left[\frac{-2r_0^2}{\omega^2}\right]\right)^{-1} Erf\left[0, \sqrt{2}\frac{z_0}{\zeta}\right]\sum_{m=0}^{m_{max}} \frac{(-\kappa)^m}{m!\sqrt{\alpha_m}\beta_m} Erf[-Z_m, Z_m]\gamma_m\right] \qquad \text{(eq. S2a)}$$

$$Z_m = \left[\frac{2}{\left(1+m+2m\frac{t}{\tau_D}\frac{\omega^2}{\zeta^2}\right)\left(1+2m\frac{t}{\tau_D}\frac{\omega^2}{\zeta^2}\right)}\right]^{0.5}\left(1 + m + 2m\frac{t}{\tau_D}\frac{\omega^2}{\zeta^2}\right)\frac{z_0}{\zeta} \qquad \text{(eq. S2b)}$$

$$\alpha_m = 1 + m\left(2\frac{t}{\tau_D}\frac{\omega^2}{\zeta^2} + 1\right) \qquad \text{(eq. S3)}$$

$$\beta_m = 1 + m\left(2\frac{t}{\tau_D} + 1\right) \qquad \text{(eq. S4)}$$

$$\gamma_m = \left(1 - exp\left[\frac{-2r_0^2}{\omega^2}\left(1 + \frac{m}{1+2m\frac{t}{\tau_D}}\right)\right]\right) \qquad \text{(eq. S5)}$$

$$Erf[x_1, x_2] = \frac{2}{\sqrt{\pi}}\int_{x_1}^{x_2} e^{-t^2}\, dt \qquad \text{(eq. S6)}$$

where ΔF_{max} is the final value of $\Delta F(t)$ and corresponds to the mobile fraction of fluorescent macromolecule under the assumption of total photobleaching of the immobile fraction; κ is the depth of photobleaching parameter and, in the model, is the exponential decay exponent of the fluorophore concentration in the center of the focused region, valued right before fluorescence recovery begins to be recorded; ω and ζ are the horizontal and vertical e^{-2} decay distances of the excitation beam profile, r_0 and z_0 are the radius and vertical half length of the assumed detection cylinder, with r_0 = 322 nm and z_0 = 1344 nm, as estimated from the fit of a 3-dimensional Gaussian function to the intensity profile of *z*-stacked *x*-*y* scans of immobilized 200 nm-diameter fluorescent beads; ω was set to be equal to r_0, and ζ was estimated as $\zeta = 8\ \omega$ according to the analysis of photobleaching profiles of TRF2-$(T_2AG_3)_{19}$ droplets formed in presence of 3'FAM-$(T_2AG_3)_{19}$. Finally, τ_D is the time for getting a root mean square displacement on the *xy* plane equal to ω^2 through 2-D translational diffusion with the diffusion coefficient *D* of the observed labeled molecule: $\tau_D = \omega^2/(4D)$.

Fitting of Eq. S2 to the data was performed through non-linear least-squares regression analysis on individual FRAP traces obtained from 3-6 different droplets. Mean values of parameters $<p>$ and their associated standard errors *s* were computed using the variance estimates from the individual fits as statistical weights w_i according to:

$$<p> = \sum_i w_i\, p_i \qquad \text{(eq. S7)}$$

$$s^2 = \frac{\frac{1}{\sum_i w_i}\sum_i w_i (p_i - <p>)^2}{\frac{\sum_i w_i^2}{(\sum_i w_i)^2} - 1} \qquad \text{(eq. S8)}$$

Phase diagram tie-lines – The concentration of TRF2 and DNA ligands in the two phases was determined employing the fluorescence intensity recorded in both phases under the confocal microscope, assuming a linear relationship between intensity and concentration and a constant molecular brightness (molar fluorescence) equal to that of the free labeled protein (Alexa Fluor 488-TRF2) or labeled DNA (3'-FAM-DNA substrates). Concentrations were computed as

$$[X_i] = \frac{(F_i - F_{bkg})}{(F_{ref} - F_{bkg})}\,[X_{tot}] \qquad \text{(eq. S9)}$$

where *X* indicates either TRF2 or DNA substrate, subindex *i* indicates the light or dense phase; F_i, F_{bkg} and F_{ref} are respectively the fluorescence intensity recorded in the *i* phase, in buffer alone and in a solution of the labeled macromolecule alone -Alexa Fluor 488-TRF2 or 3'FAM-DNA- at the same concentration and same laser power than in the final mixture; and $[X_{tot}]$ is the total concentration of the observed component (both labeled and unlabeled) in the final mixture.

Measurements of intensity in the dense phase was performed by focusing inside multiple droplets in 2-4 different 80 µm x 80 µm fields of view, at 2-10 µm from the bottom surface. Measurements in the light phase were performed by focusing in the free solution space between droplets or, for very crowded surfaces where was impossible to reliably focus in a spot without interference from neighboring droplets, in the supernatant pipetted to another cuvette after performing the measurements in the dense phase.

Framing DNA condensation in terms of polymer physics.

In the following, we wish to contextualize our experimental and computational observations in terms of the language of polymer physics, as to provide a more explicit connection between force experiments, chain condensation, and phase separation. The fundamental idea that the same forces driving chain compaction are responsible for phase separation stems directly from the Flory-Huggins model[3] and has been originally discussed in terms of nucleic acid condensation by Post and Zimm[4]. In the context of biomolecular condensates, recent experiments and simulations have confirmed that indeed the molecular interactions controlling the conformation of disordered proteins are the same interactions encoding for phase separation and can be quantitatively associated[5].

Different models can be constructed to describe this phenomenon within the framework of Flory-Huggins theories. The model proposed here has to be regarded as "a" solution, that does not pretend to cover all the possible case scenarios, but aims to provide a physics-based argument to sustain the connection between the information inferred from force spectroscopy experiments and phase-separation. Future work is required to quantitatively assess the validity of the model over other alternative descriptions.

In the spirit of the work by Post and Zimm[4], here we will describe DNA condensation by a ligand as a

modulation of the intrinsic properties of the polymer representing the nucleic acid chain. In these terms, the configuration of the polymer are dictated by two- and three-body interactions. The two-body interactions account for the physical excluded volume, repulsive electrostatics (which basically can be regarded as a virtual additional excluded volume), and the attractive interactions due to the ligand binding. A simple approximation to account for the contribution of bridging events compacting a polyelectrolyte chain has been previously described by Kundragami and Muthukumar[6], where the effective excluded volume can be defined as $v = (v_0 + \beta E_{br} c_b)$. Here v_0 is the two-body term in absence of ligand, $\beta = 1/KT$, E_{br} is the interaction energy of the ligand and DNA monomers when forming a bridge, and c_b is the concentration of the ligand. This can easily be translated in the same language used by Post and Zimm by rewriting the interaction terms as: $v = v_0\left(1 + \frac{\beta E_{br} c_b}{v_0}\right) = v_0(1 - 2\chi)$ where χ is now dependent on c_b. However, it is easy to incorporate in χ also temperature dependences and therefore in the following we will refer to χ as a generic interaction term.

Among different models, in this context, it is convenient to formulate force experiments accordingly to the model proposed by Morrison et al.[7]. Here the extensible Hamiltonian of a polymer under force is given by

$$\beta H_F = \frac{3}{2a^2}\int_0^N ds \dot{\boldsymbol{r}}^2(s) - \beta f \int_0^N ds\, \dot{\boldsymbol{z}}(s) + \Delta_2 + \Delta_3 \qquad \text{(Eq. S10)}$$

where

$$\Delta_2 = \frac{v}{2}\int_0^N ds'\delta[\boldsymbol{r}(s) - \boldsymbol{r}(s')] \qquad \text{(Eq. S11)}$$

and

$$\Delta_3 = \frac{w}{6}\int_0^N ds \int_0^N ds' \int_0^N ds'' \,\delta[\boldsymbol{r}(s) - \boldsymbol{r}(s')]\delta[\boldsymbol{r}(s') - \boldsymbol{r}(s'')] \qquad \text{(Eq. S12)}$$

With $\beta = 1/KT$, N being the number of monomers in the polymer chain, z the direction along which the f force is aligned, Δ_2 and Δ_3 the contribution of two- and three-body interactions (v_0 and w_0 respectively). The first term of the Hamiltonian describes the ideal chain, whereas the second term introduces the extension of the polymer along the z-axis. The third term describes two-body interactions and, in the spirit of the Post and Zimm work, these interactions will reflect not only the repulsive nature of the electrostatic in the DNA as well as the intrisic rigidity (persistence length), but also the attractive contribution induced by the binding of proteins.

A self-consistent equation for the extension of the polymer associated with βH_F is given by:

$$\lambda^2 - 1 = \left(\frac{3}{2\pi}\right)^{3/2}\frac{v\sqrt{N}}{\lambda^3}\int_\delta^1 \frac{1-u}{\sqrt{u}} e^{-\frac{N\lambda^2\varphi^2}{2}} + \left(\frac{3}{2\pi}\right)^3 \frac{w}{\sqrt{N}\lambda^6}\int_\delta^1 du_1 \int_\delta^{1-u_1} du_2 \frac{(1-u_1-u_2)(u_1+u_2)}{u_1^{3/2}u_2^{3/2}} e^{-\frac{N\lambda^2\varphi^2}{2}} \qquad \text{(Eq. S13)}$$

where φ is a dimensionless force given by $a\beta f$, δ is a cut-off parameter to ensure convergence of the integrals, and λ is the self-consistent parameter connected to the force-induced expansion of the end-to-end distance of the polymer chain. More precisely, the mean extension $\langle Z\rangle = \varphi L\lambda^2/3$ where L is the contour length of the polymer.

This self-consistent equation has up to three solutions ($\lambda_C < \lambda_B < \lambda_E$) depending on the force regime (Supplementary Figure S9A). Below a critical force φ_C the polymer chain is a collapsed globule dominated by the attractive two-body interactions and the increasing force is only moderately expanding the chain. This mirrors what was observed at low force in our experiments when the nucleic acid is bound to the protein as well as the condensed state identified in simulations. Increasing the force above φ_C leads to the appearance of two additional solutions representing a saddle point (λ_B) and an extended conformation (λ_E). The coexistence between collapsed and expanded conformations parallels what was observed in both experiments and simulations at intermediate forces. Whereas in experiments this is represented by an increase in the conformational fluctuations, the underlining mechanism is clearly highlighted in simulations (Figure 2 and Supplementary Figure S7). By further increasing the force, above a given threshold φ_E, only the most extended configuration is favored, which mirrors the final configuration state observed in simulations

and experiments at high forces.

When f is set to zero, the Hamiltonian simplifies to one of a polymer chain with two- and three- body interactions in absence of force:

$$\beta H_0 = \frac{3}{2a^2}\int_0^N ds\dot{\boldsymbol{r}}^2(s) + \Delta_2 + \Delta_3 \qquad \text{(Eq. S14)}$$

whose solutions can be described by the self-consistent equation[8]:

$$\alpha^2 - 1 = \frac{4}{3}\left(\frac{3}{2\pi}\right)^{3/2}\frac{v\sqrt{N}}{\alpha^3} + \left(\frac{3}{2\pi}\right)^3\frac{B\,w}{2\alpha^6} \qquad \text{(Eq. S15)}$$

Here B is equal to $\frac{1}{N}\sum_{l=3}^{N}\sum_{m=2}^{l-1}\sum_{n=1}^{m-1}\frac{(l-n)}{((l-m)(m-n))^{3/2}}$.

The equivalent free energy of the single chain in solution can be written also as[8]:

$$\beta F_{chain} = \frac{3}{2}(\alpha^2 - 2\ln\alpha) + \left(\frac{3}{2\pi}\right)^{3/2}\frac{v\sqrt{N}}{\alpha^3} + \left(\frac{3}{2\pi}\right)^3\frac{B\,w}{2\alpha^6} \qquad \text{(Eq. S16)}$$

When mixing multiple chains, the free energy of the solution can be written in terms of the number of solvent and polymer molecules n_1 and n_2 and their corresponding volume fractions v_1 and v_2:

$$\beta F_{mix} = n_1\ln v_1 + n_2\ln v_2 + \chi n_1 v_2 \qquad \text{(Eq. S16)}$$

In the work of Post and Zimm[4] the two free energies are then combined as:

$$\beta F_{tot} = \beta F_{mix} + n_2\,\beta F_{chain} = n_1\ln v_1 + n_2\ln v_2 + \chi n_1 v_2 + n_2\left(\frac{3}{2}(\alpha^2 - 2\ln\alpha) + \left(\frac{3}{2\pi}\right)^{3/2}\frac{v_0(1-2\chi)\sqrt{N}}{\alpha^3} + \left(\frac{3}{2\pi}\right)^3\frac{B\,w}{2\alpha^6}\right) \qquad \text{(Eq. S17)}$$

The phase separation is obtained by equating the chemical potential in the light and dense phase (Supplementary Figure S9B), with the chemical potentials of the two phases being:

$$\beta(\mu_2 - \mu_{20})' = \beta(\mu_2 - \mu_{20})'' \qquad \text{(Eq. S18a)}$$

and

$$\beta(\mu_1 - \mu_{10})' = \beta(\mu_1 - \mu_{10})'' \qquad \text{(Eq. S19a)}$$

Here, the sub-indexes 1 and 2 refers to the solvent and polymer, μ_{20} and μ_{10} are the chemical potentials of reference of the pure species, and the upper indexes refer to the values in the two phases.

The balance of chemical potential enables reconstructing a phase-diagram of the polymer concentration as function of χ. It is important to notice that this representation (as in the original Post and Zimm work[4]) does not account for the ligand concentration dependence of χ, nor for the volume fraction occupied by the ligand in solution nor for the different modes of binding. This does not mean that the general hypothesis is wrong, as shown by the simulations in the present work, where the same set of interactions dictates both the collapse of the single chain (and its response to force) and the phase separation of multiple chains. A quantitative description of the phenomenon requires to expand the model accounting for these additional elements, which can be derived in the context of a three-component Flory-Huggins scheme. Advancement in the single-molecule spectroscopy of nucleic acid condensation has led to develop new models that accounts for the effect of surface tension and capillary forces (which can bring together distant parts of the nucleic acid[9]) as well as the contribution of pre-wetting near a surface[10].

Supplementary references.

1 Schuler, B., Müller-Späth, S., Soranno, A. & Nettels, D. in *Intrinsically disordered protein analysis* 21-45 (Springer, 2012).

2 BLONK, J. C. G., DON, A., Van AALST, H. & BIRMINGHAM, J. J. Fluorescence photobleaching recovery in the confocal scanning light microscope. *Journal of Microscopy* **169**, 363-374, doi:https://doi.org/10.1111/j.1365-2818.1993.tb03312.x (1993).

3 Rubinstein, M., & Colby, R. H. . *Polymer physics*. (Oxford: Oxford University Press, 2003).

4 Post, C. B. & Zimm, B. H. Theory of DNA condensation: collapse versus aggregation. *Biopolymers* **21**, 2123-2137, doi:10.1002/bip.360211104 (1982).

5 Martin, E. W. *et al.* Valence and patterning of aromatic residues determine the phase behavior of prion-like domains. *Science* **367**, 694, doi:10.1126/science.aaw8653 (2020).

6 Kundagrami, A. & Muthukumar, M. Theory of competitive counterion adsorption on flexible polyelectrolytes: divalent salts. *J Chem Phys* **128**, 244901, doi:10.1063/1.2940199 (2008).

7 Morrison, G., Hyeon, C., Toan, N. M., Ha, B.-Y. & Thirumalai, D. Stretching Homopolymers. *Macromolecules* **40**, 7343-7353, doi:10.1021/ma071117b (2007).

8 Huihui, J., Firman, T. & Ghosh, K. Modulating charge patterning and ionic strength as a strategy to induce conformational changes in intrinsically disordered proteins. *J Chem Phys* **149**, 085101, doi:10.1063/1.5037727 (2018).

9 Quail, T. *et al.* Force generation by protein–DNA co-condensation. *Nature Physics* **17**, 1007-1012, doi:10.1038/s41567-021-01285-1 (2021).

10 Zhao, X., Bartolucci, G., Honigmann, A., Jülicher, F. & Weber, C. A. Thermodynamics of wetting, prewetting and surface phase transitions with surface binding. *New Journal of Physics* **23**, 123003, doi:10.1088/1367-2630/ac320b (2021).

Table S1. List of primers used for cloning and site-specific mutagenesis.

Primer	Sequence
hTERF2-F	GGCTGCAGGAATTCGGAC
hTERF2-R	GGAAACTCGAGCCTGTTTCAGTTCATGCCAAG
h-TERF2-frame-F	GGAATTCGGCACAGGGACG
h-TERF2-frame-R	CGTCCCTGTGCCGAATTCC
hTERF2-Ala^{477}-F	CAAGTTCAGGCAGCTCCAGATGAAGACAG
hTERF2-Ala^{477}-R	CTGTCTTCATCTGGAGCTGCCTGAACTTG
hTERF2Δ42-F	TTATTGAATTCATGGCGGGAGGAGGCGG
hTERF2Δ86-F	TTATTGAATTCGAGGCACGGCTGGAAGAGGCAGTCAAT
pGEX-F	CCAAAATCGGATCTGGAAGTTCTGTTC
hTERF2-S294Stop-F	CCGCTGCCTCATGAACAGGGAAGGAAG
hTERF2-S294Stop-R	CTTCCTTCCCTGTTCATGAGGCAGCGG
hTERF2-A2-F	CGAATTGGATCCGCCGC
hTERF2-G86-R	GCTTACTCGAGTTAACCACAACCACGTTC
hTERF2-C148S-F	GGTTATGCAGTCTCTGTCGCGGATT
hTERF2-C148S-R	AATCCGCGACAGAGACTGCATAACC
hTERF2-C207S-F	GCTGCTGTCATTATTTCTATCAAAAACAAAG
hTERF2-C207S-R	CTTTGTTTTTGATAGAAATAATGACAGCAGC
hRap1-F	AAGTAGGATCCATGTCATTTACATTCACCAAAAGCG
hRap1-R	TAGAAGTCGACCAGAGATGCTCGGCAATTTAAGAAG
hRap1-Glu-F	TGAGAGGATCCATGGCGGAGGCGATGGATT
hRap1-Glu-R	TATCTCTCGAGTTATTTCTTTCGAAATTCAATCCTCCGAG
FAM-pUC19-842	CAGTCACGACGTTGTAAAACGACG
pUC19-929	GGAAACAGCTATGACCATGATTACG
pUC19-927-EcoRI	AGTCAGGAATTCCGAAACCCGACAGGACTATAAAGATACCAG
pUC19-927-NotI	CAAGTCGCGGCCGCCGAAACCCGACAGGACTATAAAGATACCAG
pUC19-1553r-MIul	AAAGGACGCGTGTGAAGATCCTTTTTGATAATCTCATGACCAAAATC
pUC19-1553r-NheI	AAAGGGCTAGCGTGAAGATCCTTTTTGATAATCTCATGACCAAAATC
GO-His4-MluI-F	GAGAGTACGCGTTCCTTGTGATGCTCGTCAGGG
GO-StyI-R	GAGAGACCTAGGGGTGAGCAAGAACAGGAAGG
F-T1-DH-1kb	GGATCATGTAACTCGCCTTGATCGTTGGG
R-T1-DH-NheI	GACACAGCTAGCATACCTGTCCGCCTTTCTCC
F-T1-UH-AscI	GAGAGAGGCGCGCCATGTAACTCGCCTTGATCG
R-T1-UH-1kb	CCGGATACCTGTCCGCCTTTCTCCCTTCG
$(T_2AG_3)_2$	TCAGTCTTAGGGTTAGGGTTGAGC
mixed	TCGATACACTCAGCTCAGGAGTTC

Table S2. FRAP of TRF2 in a $(T_2AG_3)_2$ and TRF2 mixture: 10 μM (mon) unlabeled TRF2 mixed with 50 nM A488-TRF2 and indicated concentration of dsDNA.

$(T_2AG_3)_2$ and TRF2 – labeled TRF2

[dsDNA] (μM bp)	recovery	*mobile fraction*	K	τ (s)
0	0.02 ± 0.01	0.03 ± 0.01	3 ± 1	131 ± 70
15	0.012 ± 0.004	0.018 ± 0.004	2.7 ± 0.2	168 ± 60
48	0.06 ± 0.02	0.07 ± 0.02	5.1 ± 0.2	51 ± 10
120	0.49 ± 0.08	0.49 ± 0.08	5.89 ± 0.02	120 ± 40
300	0.7 ± 0.1	0.8 ± 0.1	5.0 ± 0.3	170 ± 10
600	0.04 ± 0.02	0.08 ± 0.03	1.51 ± 0.02	370 ± 200

Table S3. FRAP of labeled DNA in a $(T_2AG_3)_2$ and TRF2 mixture: 50 nM labeled DNA mixed with indicated dsDNA concentration and 10 μM (mon) unlabeled TRF2.

$(T_2AG_3)_2$ and TRF2 – labeled DNA

[dsDNA] (uM bp)	recovery	*mobile fraction*	K	tau (s)
0	0.18 ± 0.04	0.19 ± 0.04	5.6 ± 0.2	15 ± 3
15	0.71 ± 0.08	0.72 ± 0.07	5.90 ± 0.03	91 ± 25
48	0.97 ± 0.03	0.97 ± 0.03	5.89 ± 0.04	49 ± 10
120	0.93 ± 0.08	0.9 ± 0.07	5.7 ± 0.1	24 ± 9
300	0.96 ± 0.02	0.96 ± 0.02	5.5 ± 0.3	15 ± 3
600	0.32 ± 0.3	0.63 ± 0.20	0.70 ± 0.20	11 ± 6

Table S4. FRAP of TRF2 in a $(T_2AG_3)_{19}$ and TRF2 mixture: 5 μM (mon) unlabeled TRF2 mixed with 50 nM A488-TRF2 and indicated concentration of dsDNA.

$(T_2AG_3)_{19}$ and TRF2 – labeled TRF2

[dsDNA] (μM bp)	recovery	*mobile fraction*	K	tau (s)
100	0.07 ± 0.03	0.16 ± 0.03	1.1 ± 0.3	120 ± 140
250	0.16 ± 0.10	0.26 ± 0.10	1.7 ± 0.2	276 ± 60

Table S5. FRAP of TRF2 in a $(T_2AG_3)_{19}$ and TRF2 mixture in presence of hRap1: 5 μM (mon) unlabeled TRF2 mixed with 50 nM A488-TRF2, 5 μM hRAP1, and indicated concentration of dsDNA.

$(T_2AG_3)_{19}$ and TRF2 + 5 μM hRap1 – labeled TRF2

[dsDNA] (μM bp)	recovery	*mobile fraction*	K	tau (s)
44	0.42 ± 0.10	0.48 ± 0.10	3.6 ± 0.9	330 ± 50
100	0.32 ± 0.04	0.45 ± 0.04	2.0 ± 0.2	176 ± 30
250	0.31 ± 0.30	0.38 ± 0.30	3.1 ± 0.3	312 ± 60

Table S6. FRAP of labeled DNA in a $(T_2AG_3)_{19}$ and TRF2 mixture: 50 nM labeled FAM-DNA mixed with indicated dsDNA concentration, 5 μM (mon) unlabeled TRF2.

$(T_2AG_3)_{19}$ and TRF2 – labeled DNA

[dsDNA]unl (μM bp)	recovery	*mobile fraction*	K	tau (s)
44	0.02 ± 0.02	0.04 ± 0.02	1.6 ± 0.3	290 ± 40
100	0.06 ± 0.01	0.08 ± 0.01	3.7 ± 0.6	570 ± 80
250	0.4 ± 0.1	0.44 ± 0.10	4.9 ± 0.8	1400 ± 200

Table S7. FRAP of labeled DNA in a $(T_2AG_3)_{19}$ and TRF2 mixture: 50 nm labeled FAM-DNA mixed with indicated dsDNA concentration, 5 μM (mon) unlabeled TRF2, and 5 μM hRap1.

$(T_2AG_3)_{19}$ and TRF2 + 5 μM hRap1 – labeled DNA

[dsDNA]unl (μM bp)	recovery	*mobile fraction*	K	tau (s)
44	0.247 ± 0.005	0.280 ± 0.004	4.72 ± 0.03	480 ± 10
100	0.58 ± 0.01	0.60 ± 0.01	5.58 ± 0.04	750 ± 20
250	0.717 ± 0.006	0.752 ± 0.005	4.61 ± 0.07	405 ± 10

Table S8. Interaction strengths used for modeling (in units of kT).

Coarse-grained simulation parameters

Bead 1	Bead 2	*Standard Strength (short/long)*	Weakened Strength (short/long)
PROTEIN	PROTEIN	0.143 / 0.07	0.136 / 0.064
PROTEIN	DNA	0.214 / 0.071	0.207 / 0.064
PROTEIN	SOLVENT	0 / 0	0 / 0
DNA	PROTEIN	0.214 / 0.071	0.207 / 0.064
DNA	DNA	0 / 0	0 / 0
DNA	SOLVENT	0 / 0	0 / 0

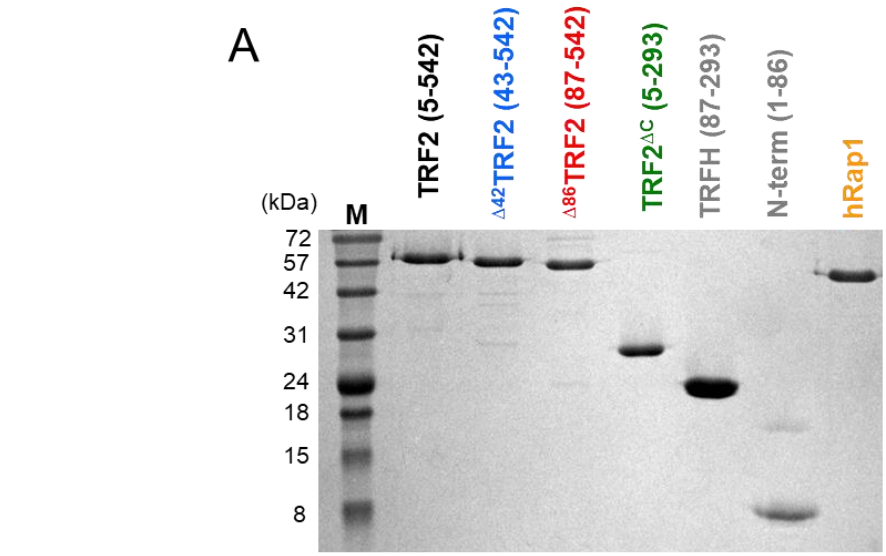

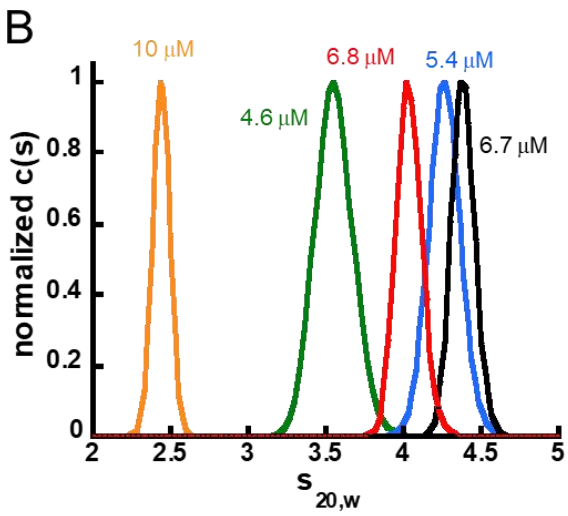

C

	$MW_{predicted}$ (kDa)	$MW_{calculated}$ (kDa)
TERF2 (5-542)	60.1	112.2
Δ42TERF2 (43-542)	56.5	101.8
Δ86TERF2 (87-542)	52.3	91.8
TERFΔC (5-293)	32.8	64.1
hRap1	44.7	44.5

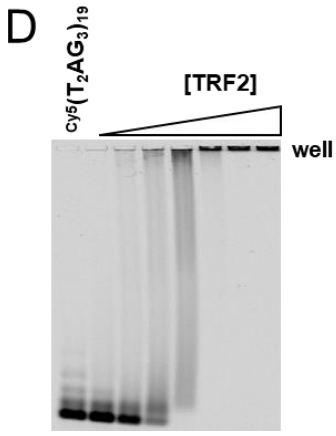

Figure S1. A. SDS-PAGE of representative protein constructs used in this study, stained with Coomassie Blue. **B**. Distribution of sedimentation coefficients from sedimentation velocity experiments of different protein constructs, at the indicated concentrations (in monomer). **C.** Molecular weights calculated from the sedimentation coefficients, compared to the ones predicted from the amino acid sequence. **D.** Binding of TRF2 to a Cy5 labeled DNA fragment containing 19 T_2AG_3 repeats, as monitored by agarose gel electrophoresis. The position of the well is indicated.

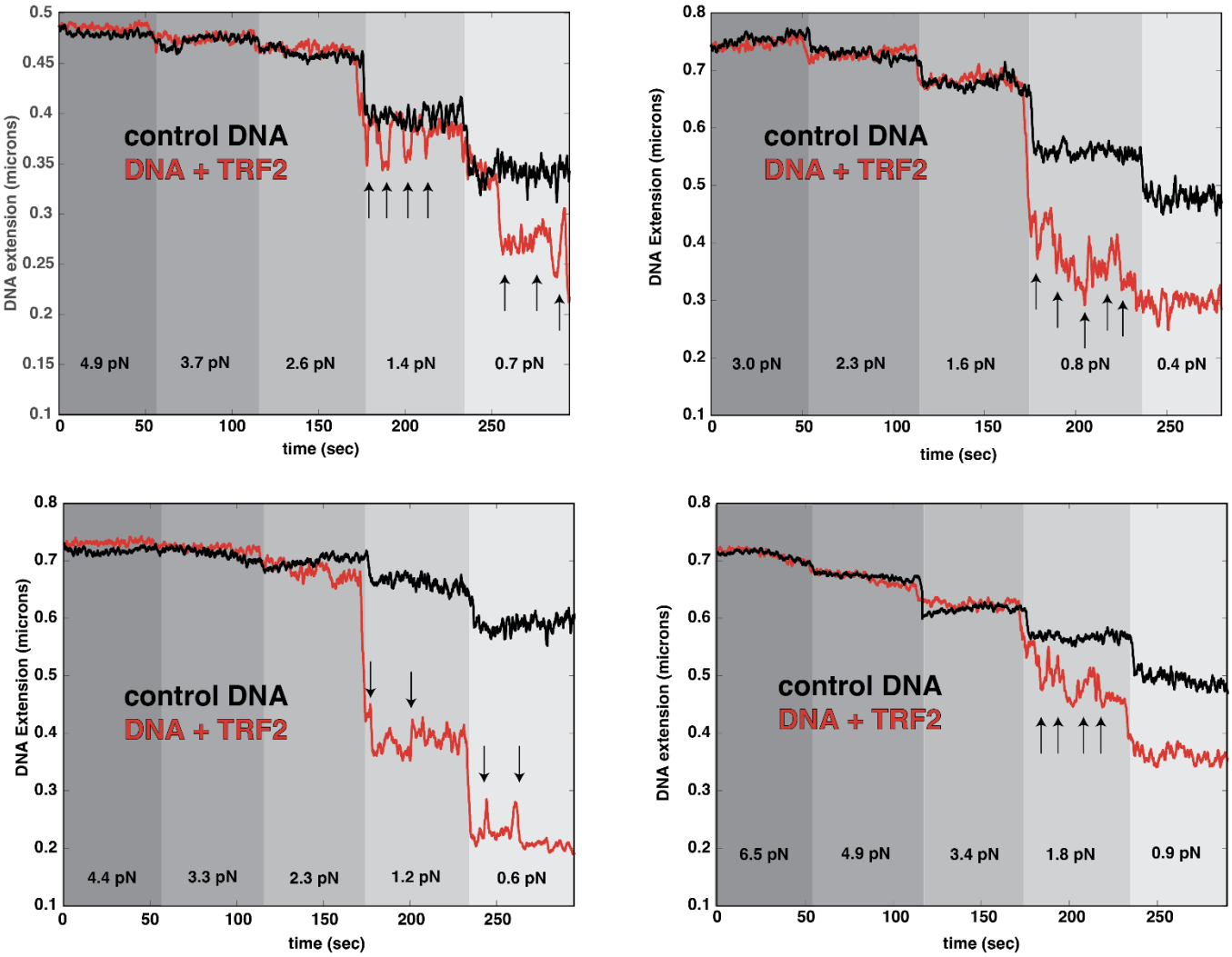

Figure S2. Examples of tethers where rapid transitions between metastable lengths are observed (i.e., hopping). The different shadings indicate different forces probed. These vary from tether to tether due to variation in the size of the magnetic beads. The black traces are controls where the DNA tether alone was taken through these force regimes. As expected, the length of the tether reduces as the force is lowered. The red traces are experiments where TRF2 is present. Features of these traces consistent with a hopping behavior are indicated with arrows.

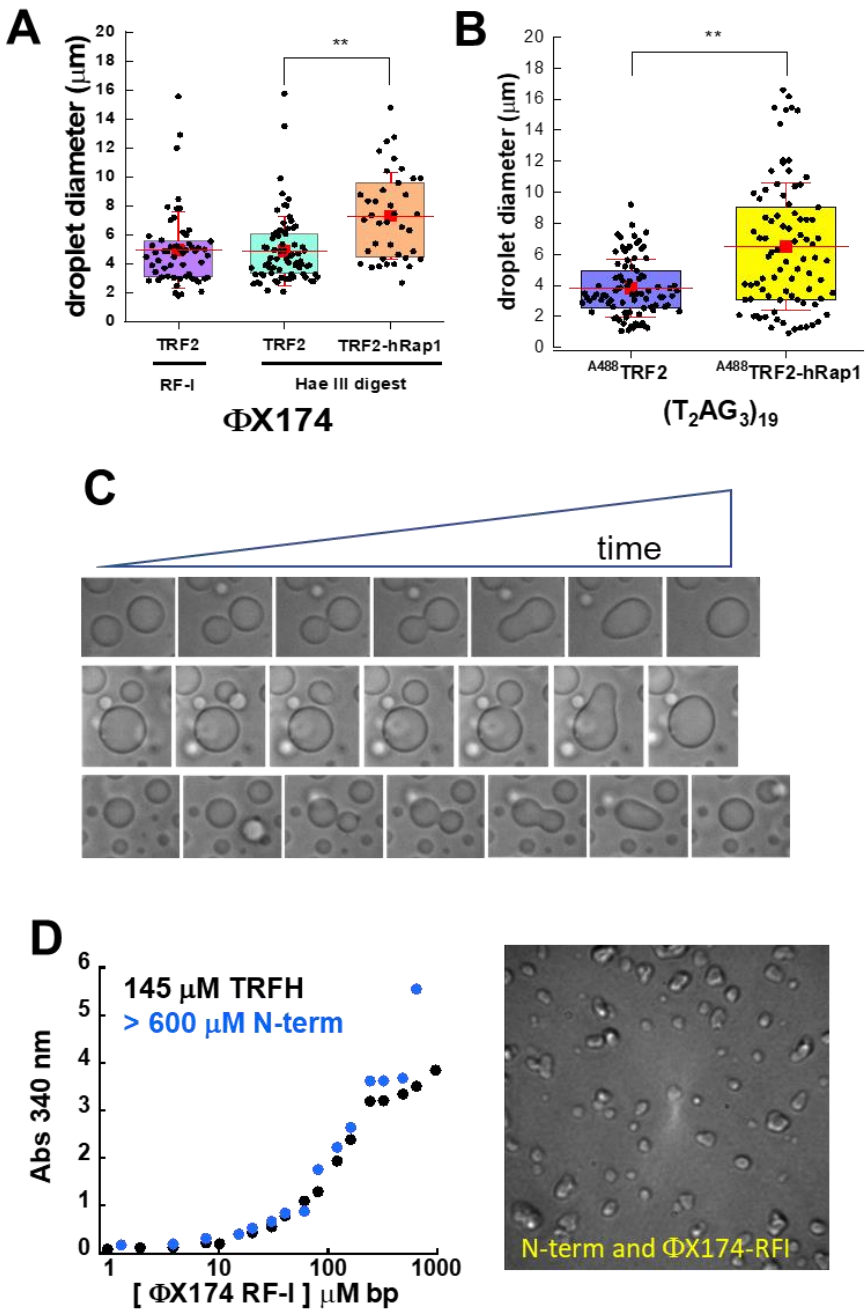

Figure S3. A. Diameter of TRF2-DNA droplets as observed by DIC, before the solution on the cover slip dried out. The diameter of the droplets formed in the presence of hRap1 is shown for comparison. **B.** Diameter of TRF2-DNA droplets in the absence and presence of hRap1, as monitored by fluorescence confocal microscopy via the fluorescence of Alexa Fluor 488 labeled TRF2. **C.** Example of TRF2-DNA droplets fusing on the surface. **D.** Mixing at high concentrations either the TRFH (black) or the N-terminal tail (blue) with ϕX174-RFI gives rise to an increase in turbidity, but corresponding objects formed in solutions are small amorphous droplets, substantially different from the round droplets observed with the full-length protein or other truncation variants.

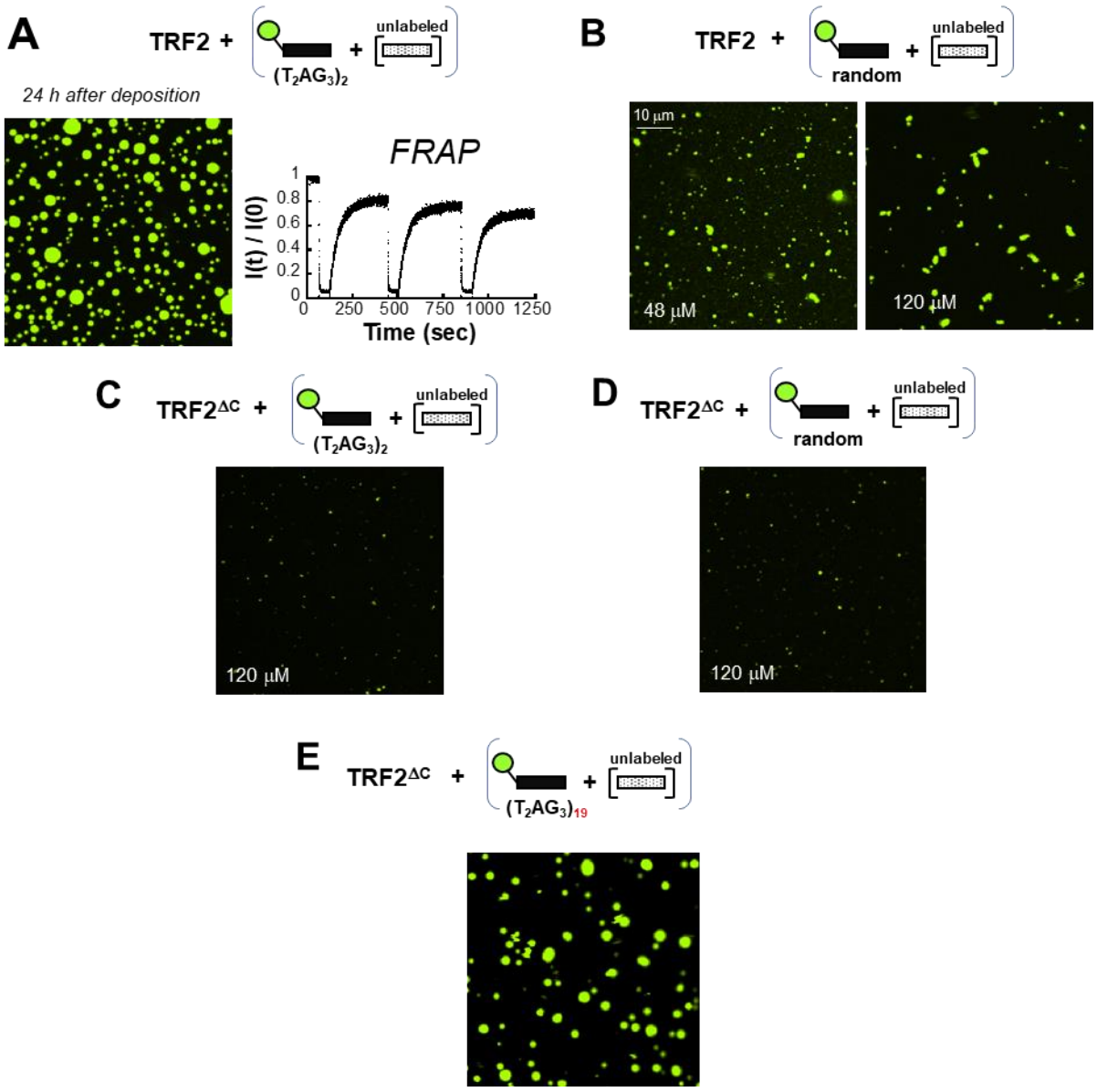

Figure S4. A. Droplets of TRF2 with a fluorescein-labeled 24 bp $(T_2AG_3)_2$ dsDNA after 24 h deposition on the surface maintain their liquid character, as monitored by FRAP. **B.** TRF2 does not efficiently form droplets with the fluorescein labeled 24 bp random DNA. **C, D.** TRF2$^{\Delta C}$ does not form droplets with either the $(T_2AG_3)_2$ or random 24 bp dsDNA at 120 μM. Few fluorescence puncta are observed, which are consistent with a significant shift of phase boundaries toward higher nucleic acid concentrations and a strong reduction of phase separation propensity. **E.** TRF2$^{\Delta C}$ forms droplets with the $(T_2AG_3)_{19}$ dsDNA fragment.

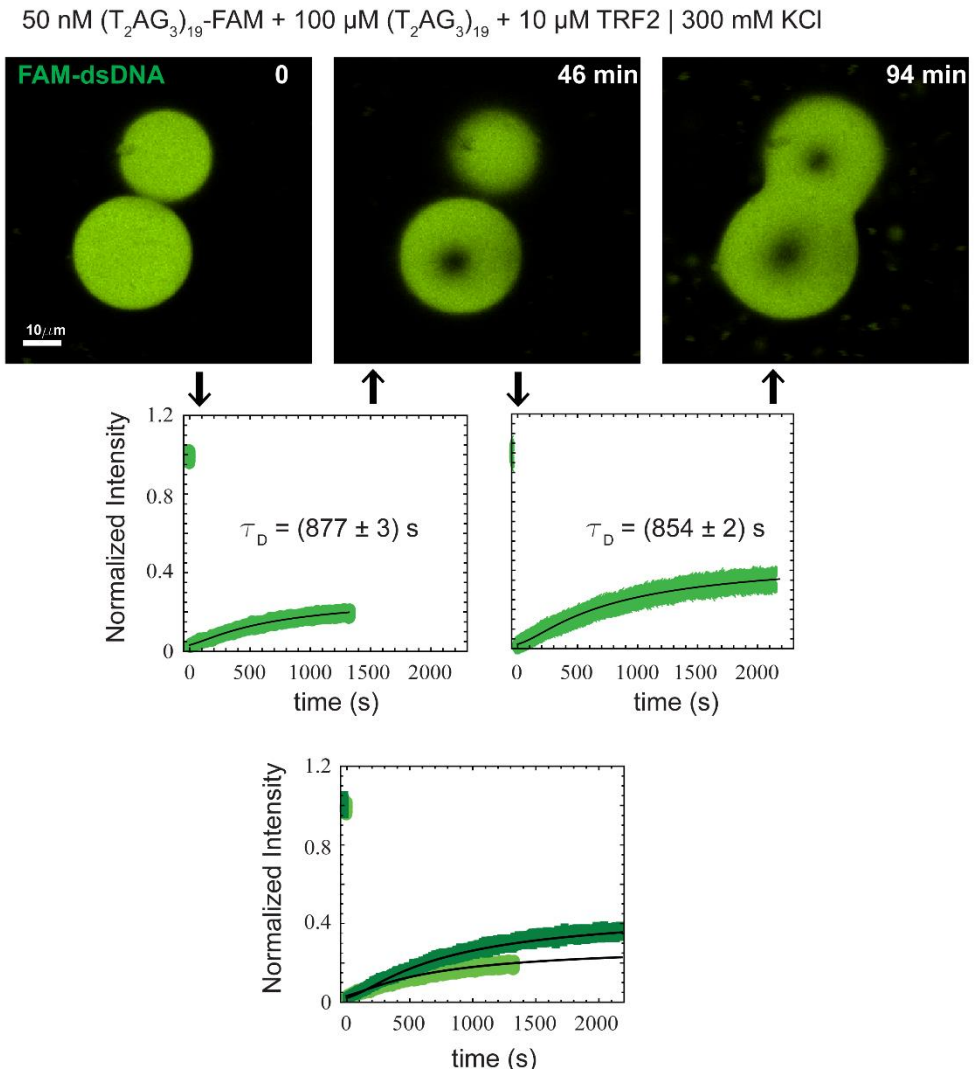

Figure S5. Fusion between droplets formed by 100 μM $(T_2AG_3)_{19}$ and 10 μM TRF2 at 300 mM KCl. A partial slow recovery after photobleaching is observed in each droplet with a characteristic time of approximately 800-900 seconds. Though fusion duration is likely to be slowed down by interaction with the surface, this observation suggests that despite the slow and partial recovery of each droplet, the two can still fuse together.

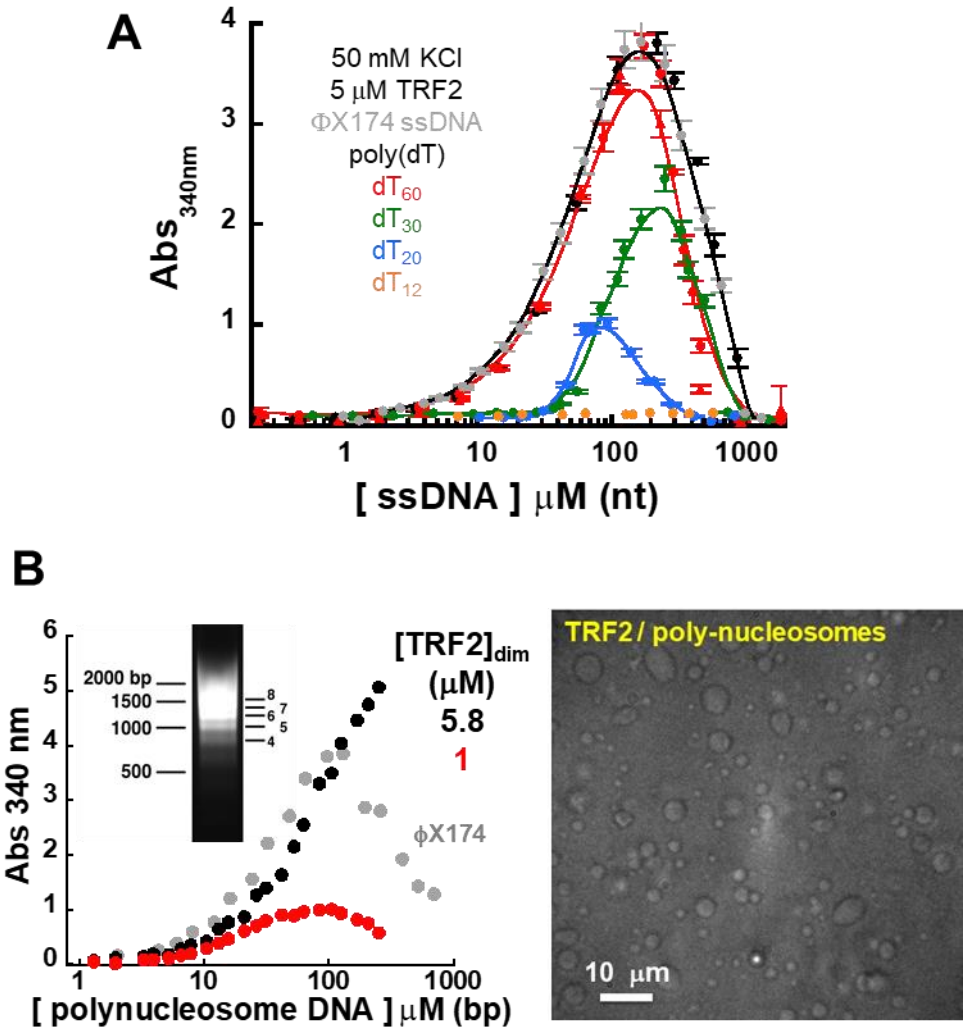

Figure S6. A. Absorbance scattering of TRF2 (5 μM dimer) and ssDNA of different lengths. **B.** Absorbance scattering and DIC imaging indicate that formation of poly nucleosomes does not suppress the ability of TRF2 to phase separate with DNA.

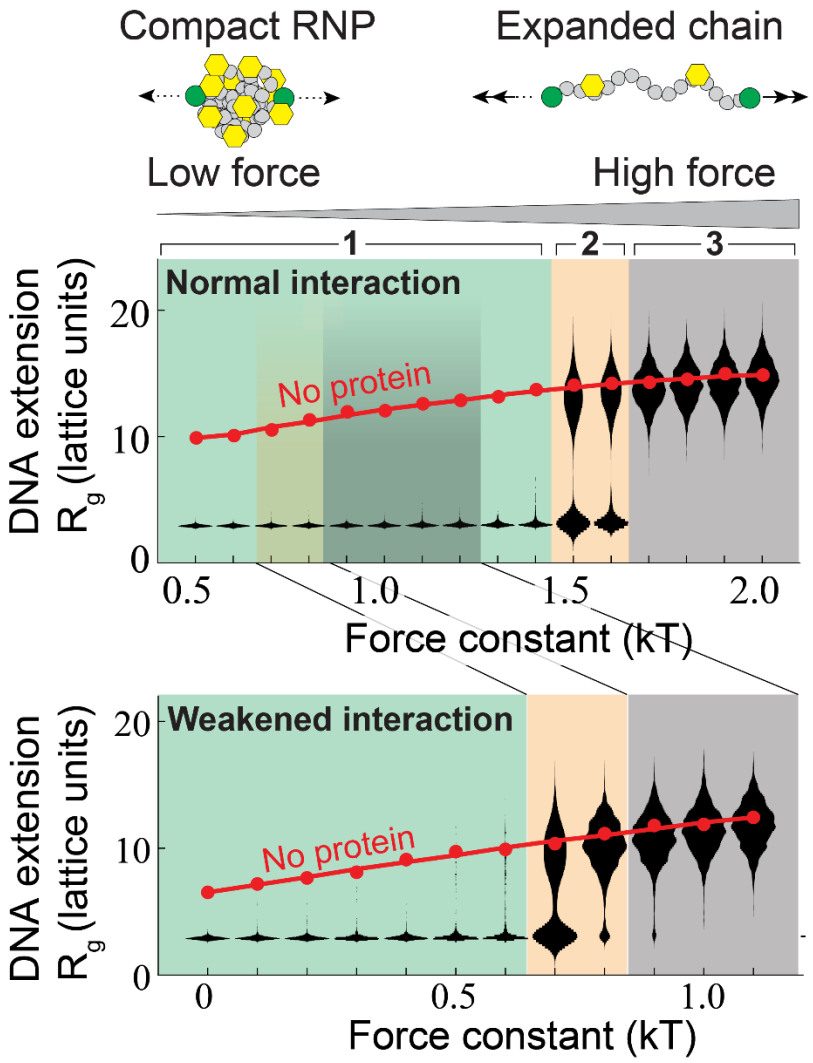

Figure S7. Comparison of DNA extension as a function of force with violin plots. Simulations of DNA expansion under constant force in absence of TRF2 (red dots) and in presence of the TRF2 (black data) with normal (top) and weakened (bottom) molecular interactions. In absence of TRF2 the DNA is expanded and adopts even more expanded configurations with increasing force. With a force constant of zero, the presence of TRF2 causes DNA compaction. As the force constant is increased, the DNA compaction transitions through a regime where the DNA is fully compact (region 1, top), a regime in which a bi-modal population of compact and extended molecules is realized by individual molecules oscillating between these two states (region 2, top), and eventually a regime in which the chain is fully extended (region 3, top). The transition between these three regions depends on the interaction strengths, which could experimentally be altered by adding hRap1 or by changing salt concentration. At high forces and at the transition large fluctuations occur and coexistence of the collapse and expanded state can be visualized, reflecting the large uncertainty observed experimentally in the transition. For convenience we refer to the molecules in our simulations as “DNA” and “TRF2”, but these are highly simplified models such that this language is provided as a rhetorical tool, as opposed to a specific description.

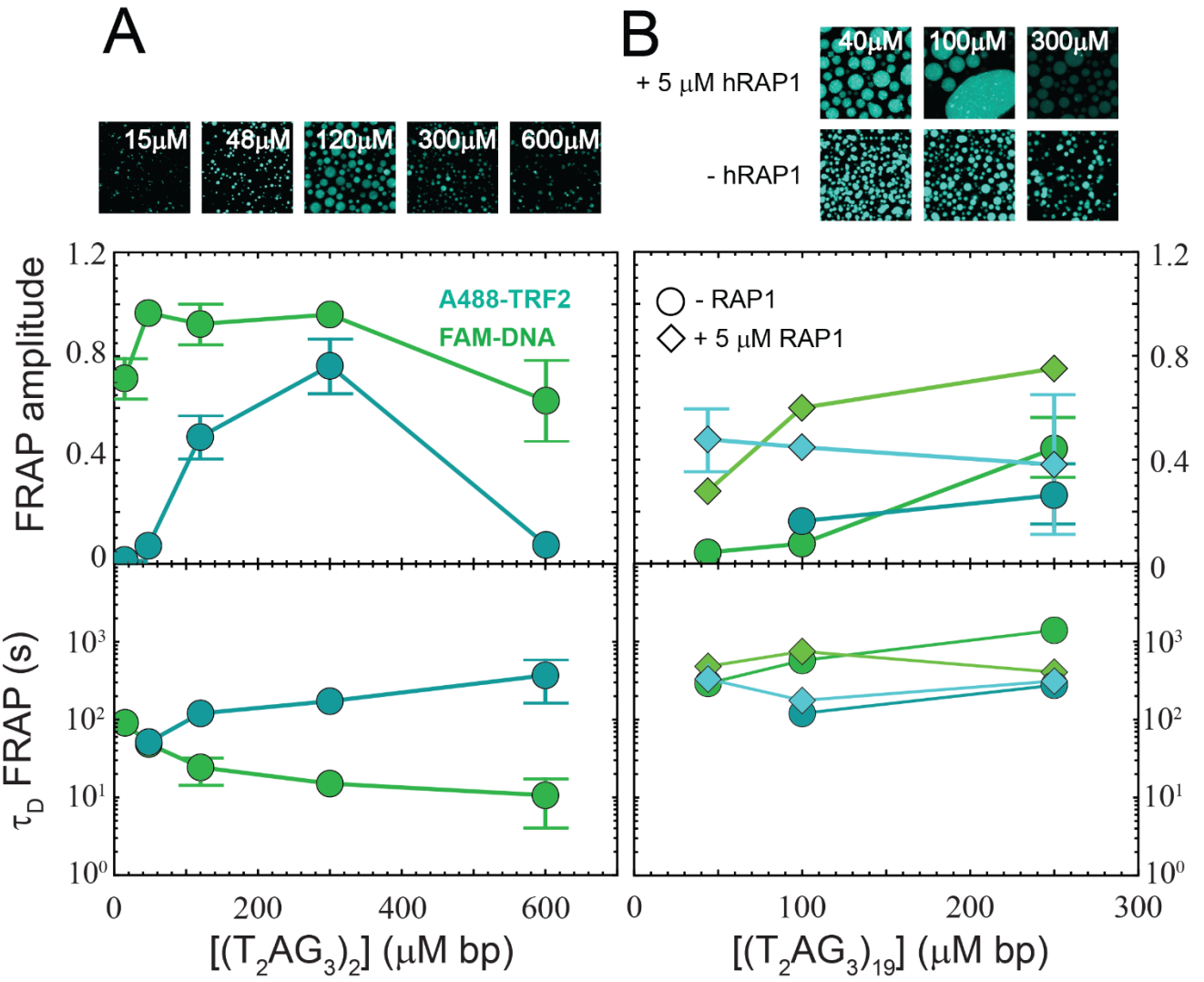

Figure S8. Fluorescence Recovery After Photo-Bleaching amplitudes and diffusion times. A. TRF2 phase separation with $(T_2AG_3)_2$ at increasing concentrations of specific DNA. Fluorescence Recovery After Photobleaching and diffusion time associated with the protein and DNA. **B.** TRF2 phase separation with $(T_2AG_3)_{19}$ at increasing concentrations of specific DNA. Error bars are standard deviations from FRAP experiments on different droplets at each condition.

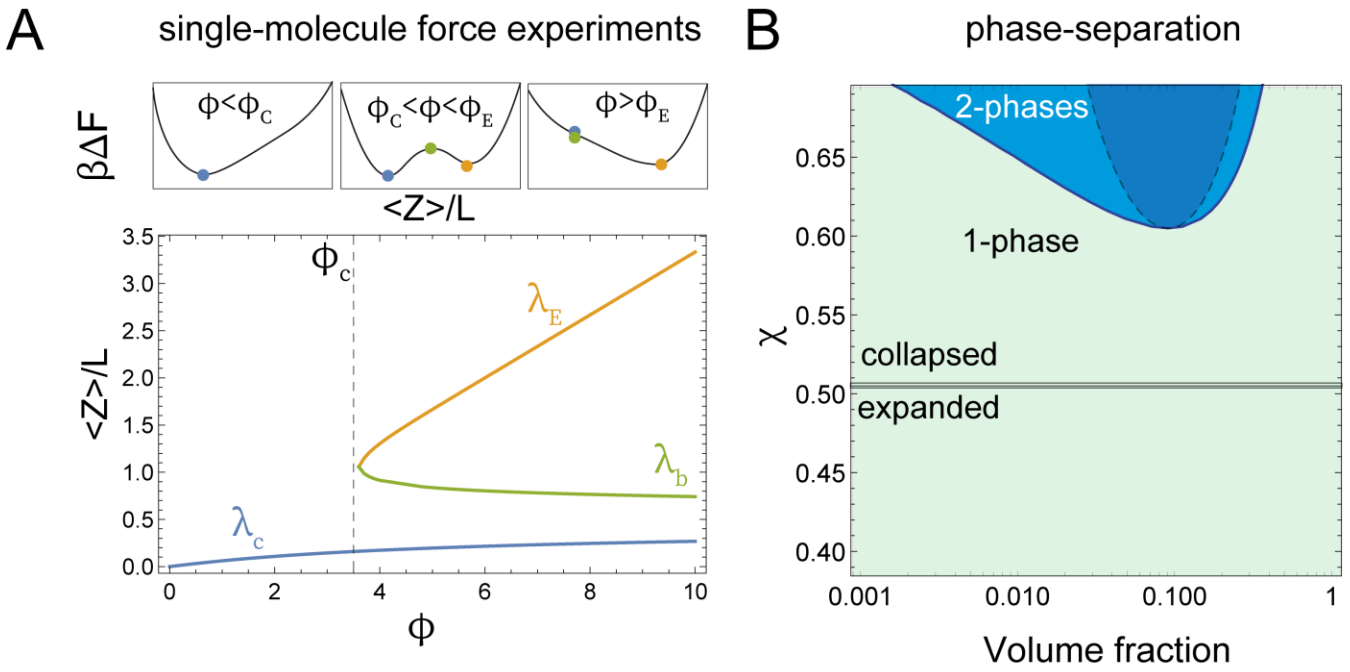

Figure S9. Polymer theory models. A. Single-molecule force experiments and simulations can be interpreted in terms of a single-chain force extension model[7] that accounts for two- and three-body interactions in the chain (see Eq. S10-S13). The mean extension of the end-to-end distance along the direction of the pulling force <Z>/L as function of the normalized force φ results in three distinct solutions λ_c, λ_b, λ_E representing a collapsed configuration, a saddle point, and an extended configuration, respectively. Increasing the force above specific threshold values (φ_C and φ_E) favors one configuration among the others (upper panels). **B**. The same interactions that control the degree of compaction as a function of the force are responsible for the phase separation of multiple polymer chains in solution according to equations S17. A critical value of χ determines whether single chains adopt extended (good solvent) or collapsed configurations (poor solvent). In poor solvent, multiple chains within certain boundaries of concentrations can partition in two distinct phases. The light blue area represents the binodal region, whereas the dark blue represents the spinodal region. All calculations performed assuming a chain constituted by 100 monomers.